J Electroceram (2011) 26:1–7
DOI 10.1007/s10832-010-9619-2

Electrical properties of $Bi_4Ti_3O_{12}$ textured by screen printing

Michael R. Winter · Christopher B. DiAntonio · Pin Yang · Tom P. Chavez

Received: 9 February 2010 / Accepted: 28 September 2010 / Published online: 19 October 2010

Abstract The focus of this work is to explore the electrical properties of bismuth titanate, $Bi_4Ti_3O_{12}$, textured through the process of screen printing. Textured BTO samples were produced using the templated grain growth technique and the electrical properties were measured both within and normal to the texture plane. The relative permittivity and polarization were determined as a function of electric field, temperature, and frequency. The electrical properties improved dramatically (P_r=25 μC/cm², $\varepsilon_r(\omega)$=1800 at 1 MHz) compared to a randomly oriented sample (P_r= 10 μC/cm², $\varepsilon_r(\omega)$=850 at 1 MHz) when measured within the texture plane. A corresponding reduction of electrical properties normal to the texture plane was observed (P_r= 2 μC/cm², $\varepsilon_r(\omega)$=300 at 1 MHz). The electrical properties of bismuth titanate textured by screen printing compare favorably to other texture-inducing techniques such as tape casting and hot forging.

Keywords Bismuth titanate · Lead-free · Texture · Screen printing · Dielectric · Ferroelectric · Electrical properties

1 Introduction

Lead-based ferroelectrics are the materials of choice for multiple applications due to their excellent electrical properties and the ability to be tailored to a variety of specific applications through compositional adjustment. Increasing environmental restrictions and manufacturing costs from lead use in industry have galvanized research seeking alternative materials with equivalent properties and have led to a renewed interest in replacing the current ferroelectrics with lead-free materials. Layer-structured perovskites offer a rich variety of potential alternatives, particularly the bismuth layered and alkali niobate-based solid solution ferroelectrics; however, these materials generally do not have sufficient electrical properties to displace the current systems [1, 2].

Texture induced by high shear forming techniques, such as tape casting, hot forging, and screen printing, has improved the electrical properties of several lead-free systems [3–16]. In certain systems, texturing results in electrical properties that approach those of current lead-based systems, making these textured materials potential candidates for lead-free devices [17]. The improvement in electrical properties of layer-structured ferroelectrics textured through tape casting and hot forging have been well documented, but it has not been determined if comparable improvements may be realized through screen printing. Screen printing offers unique advantages over tape casting such as the ability to print complex patterns and integrated fabrication.

Bismuth titanate, $Bi_4Ti_3O_{12}$ (referred to as BTO in this paper), is a well characterized layer-structured system and has been textured using a variety of techniques [3, 5–12, 15, 18]. Texture is generally achieved by introducing seed crystals into a matrix of equiaxed powder, although this step is not necessary in the case of hot forging. Several techniques have been developed to grow high aspect ratio BTO seeds up to 50 μm in size, which are easily oriented during high shear processing [6, 7, 11, 12, 14, 18–22]. The seeds grow as the matrix powder is consumed during sintering, leading to a crystallographically oriented, dense sample. This technique is known as templated grain growth, TGG. As the polarization axis of BTO lies within the

M. R. Winter (✉) · C. B. DiAntonio · P. Yang · T. P. Chavez
Sandia National Laboratories,
Albuquerque, NM, USA
e-mail: mrwinte@sandia.gov

texture plane, the effect of texture on the electrical properties due to orientation is readily apparent [19, 23].

This work examines the effect of crystallographic texture on the electrical properties of bismuth titanate formed by screen printing. Electrical properties were measured within the texture plane as well as normal to the texture plane and compared to the electrical properties of BTO textured by hot forging and tape casting.

2 Experimental procedure

The preparation of BTO seed crystals, formulation of screen printing ink and the screen printing process are described in detail in previous work [18]. Briefly, phase pure bismuth titanate seeds were grown using molten salt synthesis and equiaxed BTO powder, with 10 weight percent excess bismuth oxide, was formed through standard mixed oxide processing. Screen printing ink was prepared using a commercial vehicle and about 90 weight percent ceramic with small adjustments (2–3%) to achieve proper ink rheology. The ceramic component in the inks containing seeds was comprised of 10 weight percent seeds to 90 weight percent equiaxed powder.

The ink was printed on a Mylar sheet (Mylar A-200, DuPont Teijin Films) taped to an alumina wafer (99.5% Alumina M12546, Coorstek) and dried at 130°C for 15 min. After the initial print, Mylar shims were used to support the screen from beneath, allowing printing of multiple layers to build a pad approximately 0.8 mm thick. The pad was gently peeled from the Mylar, sealed in a platinum crucible, and sintered for 4 h between 1130°C and 1140°C, which is very close to the melting point. Bismuth loss was minimized by using a sealed crucible and the excess bismuth from the equiaxed powder. Electrical properties are highly dependent on density; therefore, the sintering conditions were increased to just below the melting temperature, but have not been studied in detail to achieve the optimum microstructure.

The rapid movement of the squeegee generates high shear forces within the ink as the pad is printed, orienting the seeds and allowing the TGG process to occur during sintering. The crystallographic texture generated by this process is very high (Lotgering factor of 0.98–0.99 and a multiples of a random distribution value of >5 along the (008) direction at 0° chi tilt) and equal to that generated using hot forging and tape casting, allowing a comparison of electrical properties to literature.

Electrical testing samples were diced from the sintered pads. Samples measured along the c-axis were approximately 0.7 mm thick and those within the a-b plane approximately 2.5 mm thick. The samples are highly textured along the c-axis, but have a rotational degree of freedom within the a-b plane. Figure 1 shows a schematic (not to scale) of the sample fabrication process and the orientation axes used when describing the electrical results.

Diced samples were polished to 800 grit and platinum electrodes were sputtered (K550X Sputter Coater, Quorum Emitech, UK) to create electrical contacts. Any platinum deposited along the sides of the sample was removed by a final polish to prevent electrical shorting.

High field polarization as a function of electric field was measured using a modified Sawyer-Tower circuit built in-house. The sample was mounted in the test fixture and placed in a jar containing silicon oil (561 Transformer Fluid, Dow Corning Corp., MI) to prevent shorting. The jar was placed in an environmental chamber (EC1A, Sun Electronic Systems, FL) with the capacity to cool with liquid nitrogen and resistively heat. The electric field was applied with a high voltage amplifier (10/10B, Trek, NY). Weak field relative permittivity and loss tangent measurements were performed using an impedance analyzer (4194A, Agilent, CA). The sample was placed in the test fixture located inside an 1100°C clamshell furnace which was heated during the measurements.

Several test samples were used during the course of this work and small variations in electrical properties were observed. These variations are likely due to processing adjustments, such as higher sintering temperatures and higher solids loading, leading to lower observed residual porosity. It was not possible to accurately measure the final density of the screen printed samples given the small sample thickness. To fully explore the potential of screen printing, the technique needs to be optimized, as the electrical properties are affected by the sample density and microstructure. The results presented are intended as a preliminary comparison of screen printing to other texture-inducing techniques, demonstrating the viability of screen printing to produce equivalent improvements in the electrical properties of textured BTO.

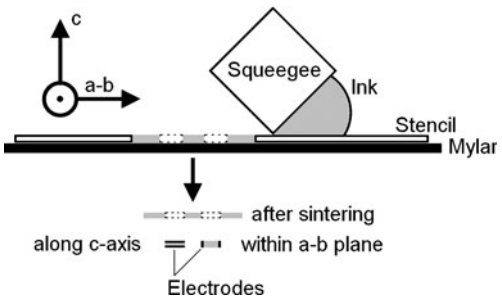

Fig. 1 Schematic of the screen printing technique showing the orientation of the samples diced from the sintered pad within the a-b plane and along the c-axis

3 Results and discussion

Textured samples were examined both within the a-b plane (within the texture plane) and along the c-axis (normal to the texture plane), as referenced in Fig. 1. As the polarization lies along the a-direction about 5° off of the a-axis toward the c-axis, one would expect that the electrical properties within the a-b plane would show a significant improvement compared to a random, polycrystalline sample and those along the c-axis would show a decline compared to a random sample. Because the dipole moment remains random within the a-b plane, one would expect the polarization to be well below that of single crystal BTO (50±10 μC/cm²) within the a-b plane; however, the polarization along the c-axis is expected to be fairly close to the single crystal value (4±0.1 μC/cm²) [19].

3.1 Polarization response to electric field

The effect of drive voltage on the polarization of textured samples within the a-b plane is shown in Fig. 2, with the sinusoidal drive voltage applied as a positive voltage initially.

The remanent polarization was improved when measured within the a-b plane compared to a randomly oriented sample (9.3 μC/cm², 12.8 μC/cm², respectively) [3, 24]. As the drive voltage was increased to 7 kV, the sample began to reach saturation and would likely not have increased significantly. Typical remanent polarization for screen printed samples ranged from 20–30 μC/cm², while previous hot forging work gives higher and lower values (37 μC/cm², 14 μC/cm², respectively) [3, 5]. It is somewhat problematic to directly compare these results to previous work, as measurement frequencies are not always consistent and the electrical properties of BTO show significant frequency dependence. Differences in processing conditions, degree of texture, and final density further complicate comparisons as variations in the defect chemistry or residual stresses may be present, altering the electrical properties of the material. Scanning electron micrographs show some residual porosity in the sample, which would decrease the remanent polarization over a fully dense sample. However, the remanent polarization is significantly improved compared to a randomly oriented sample. The screen printed samples experienced 100 kV/cm without breakdown, which is also comparable to previous work using other texturing methods.

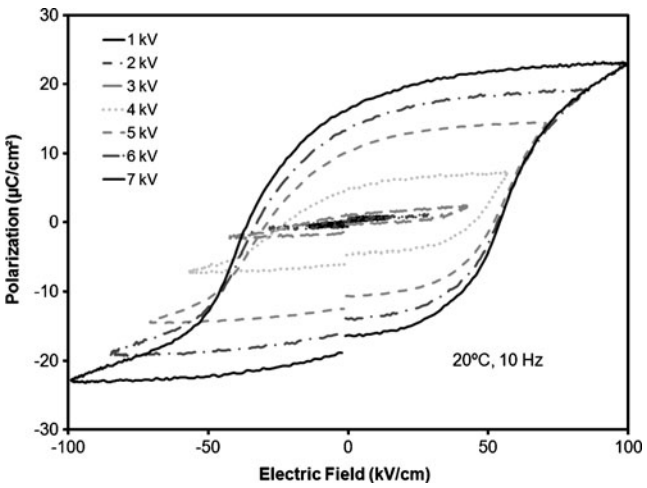

Fig. 2 Effect of drive voltage on the polarization within the a-b plane measured at 20°C and 10 Hz

The P-E loops are asymmetric, being somewhat pinched under negative electric fields compared to positive electric fields, especially at lower drive voltages. The coercive field was approximately 50 kV/cm, although the P-E loops were not centered about the origin and showed some dependence on electric field history. For example, when the samples experienced negative electric fields initially, the loops were shifted in the negative direction and were pinched when experiencing positive electric fields. This dependence is likely due to induced changes in defect chemistry of BTO under an electric field. Previous work has shown that the defect chemistry of BTO is complex and sensitive to impurity levels, which may explain the asymmetry [21, 25].

The internal bias, defined as the electric field necessary to center the loops about at the origin along the electric field axis, has been described by previous work and may be caused by a variety of phenomena such as grain boundary second phases and defects due to vacancies or atomic substitutions [26, 27]. These phenomena have resulted in effects such as domain wall pinning, aging and changes in hysteresis behavior. The mechanisms creating the internal bias observed in this work were not explored, but remain an issue of further study as the electrical properties should remain consistent regardless of electric field history.

The effect of drive voltage (lower due to the evaluation of thinner samples) on the polarization of textured samples along the c-axis is shown in Fig. 3.

As expected, the polarization was much lower along the c-axis compared to a randomly oriented sample. The remanent polarization was about 2 μC/cm², although that value is somewhat lower than previous work and single crystal values, possibly due to porosity within the sample [3, 19]. The values measured in this work are similar to previous work and demonstrate the expected trends. The coercive field was 38 kV/cm as the electric field increased, but shifted to –17 kV/cm as the field was reversed. At low drive voltages, the loops were fairly symmetric. As the drive voltage increased, the P-E loops became more asymmetric, which is likely due to the complex crystal structure and internal defect chemistry of BTO.

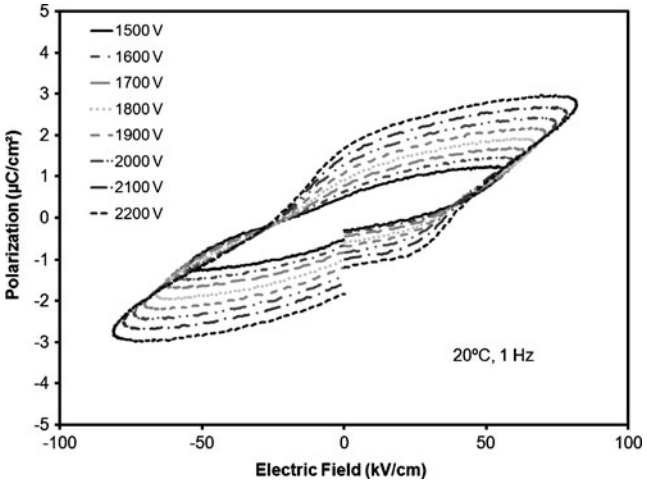

Fig. 3 Effect of drive voltage on the polarization along the c-axis measured at 20°C and 1 Hz

3.2 Frequency-dependent polarization as a function of electric field

The P-E loops were measured at several frequencies within the a-b plane of the textured sample. The room temperature results are shown in Fig. 4.

At room temperature, the P-E loops are fairly similar at higher frequencies, but broaden below 5 Hz, indicating the onset of conduction mechanisms. While crystalline texturing of BTO improves electrical properties by orienting dipole moments within the a-b plane, it also increases conduction through crystalline orientation and affects electrical properties, Several conduction mechanisms have been proposed, including p-type conductivity through acceptor impurities and cation vacancies, as well as over-bonding of the bismuth ions [25]. The grain size may also affect conduction by altering the defect structure [25]. The defect chemistry was not explored, but remains an important consideration when evaluating electrical properties.

The loops show a slightly higher remanent polarization than previously shown, likely due to improvements in the sample fabrication resulting in less residual porosity. The coercive field remains consistent and the sample shows no signs of dielectric breakdown under strong electric fields. The loops are somewhat asymmetric, indicating that the polarization behavior is dependent on electric field history and the defect chemistry of BTO is likely affecting the response, as discussed previously.

The P-E loops were measured at several frequencies along the c-axis of the textured sample. The room temperature results are shown in Fig. 5.

The frequency dependence of the P-E loops along the c-axis is consistent with those within the a-b plane, although the polarization is much lower. This is an expected result as the dipole moment lies nearly within the a-b plane. Below about 5 Hz, the loops become lossy and by 0.1 Hz the conduction mechanisms are very active, leading to a nearly oval loop. The very large polarization is due to conduction within the sample. The remanent polarization (~2 μC/cm²), and coercive field remain consistent with the loops generated by varying the drive voltage and are consistent with previous work in the literature.

3.3 Temperature-dependent polarization as a function of electric field

The P-E loops measured within the a-b plane at temperatures above about 30°C show increasing conduction, manifested as broadening loops with increasing temperature, shown in Fig. 6.

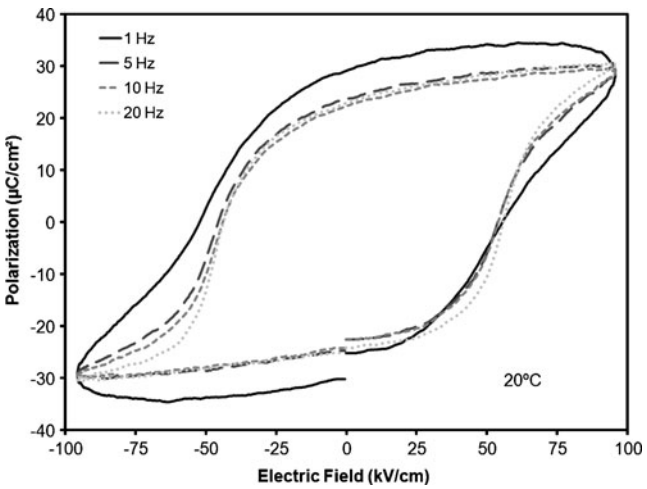

Fig. 4 Effect of frequency on the polarization within the a-b plane of a textured sample measured at 20°C

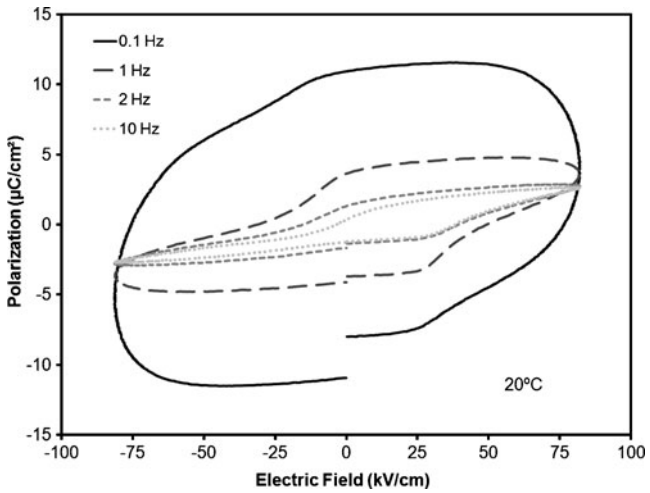

Fig. 5 Effect of frequency on the polarization along the c-axis of a textured sample measured at 20°C

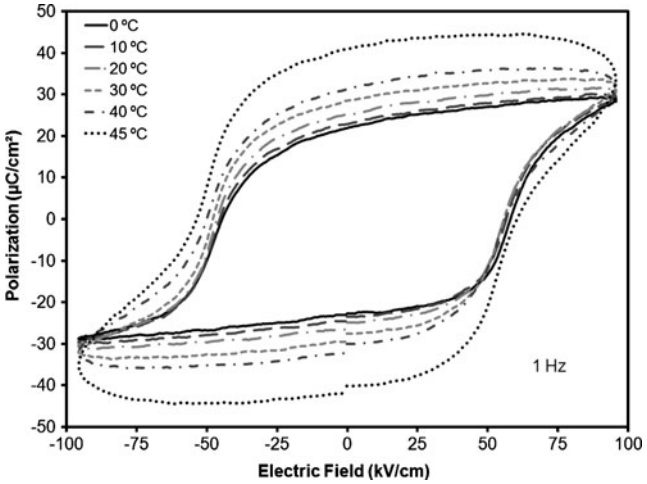

Fig. 6 Effect of temperature on the polarization within the a-b plane of a textured sample measured at 1 Hz

The loops of the textured samples began to broaden at temperatures below that of the random sample, indicating that the conduction mechanisms were also enhanced through the texturing process. The sample showed no signs of dielectric breakdown at fairly high electric fields and shows a similar coercive field (~50 kV/cm) and remanent polarization (~25 μC/cm²) as previous tests. The remanent polarization is slightly higher for this sample, which is likely due to improved sample fabrication and consequently less residual porosity. The coercive field and remanent polarization are comparable to previous work texturing BTO with other processing techniques. Polarization is also expected to improve with temperature as dipole reorientation is facilitated by thermal energy, although it is difficult to quantify this effect alone as conduction mechanisms are also concurrently enhanced by thermal energy.

The temperature dependence of the P-E loops measured along the c-axis is shown in Fig. 7.

At the lowest measured temperatures, the loops overlap, indicating that any conduction mechanisms have reached a steady state. The loops are very asymmetric and nearly linear as the sample is cycled through negative electric fields, indicating that the domain orientation in response to electric field is complex. This effect, however, becomes less prominent as the temperature increases, facilitating domain reorientation and electrical conduction. Previous work on hot forged BTO yielded symmetric polarization loops at room temperature along the c-axis [3]. Those measurements were conducted at 50 Hz however, highlighting the fact that direct comparison across texture techniques can be difficult. Additionally, the electrical properties of BTO, especially textured BTO, are strongly dependent on measurement frequency. The coercive field is quite different as the drive voltage is cycled through the test. As with the a-b plane polarization loops, the c-axis loops begin to open at temperatures above about 30°C, indicating increased conduction within the sample. As the temperature increases, the loops become more symmetric, demonstrating that the defect chemistry is temperature dependent.

3.4 Weak-field relative permittivity and loss tangent as a function of temperature and frequency

Weak-field relative permittivity measurements were performed from room temperature to 700°C at measurement frequencies of 1 kHz, 10 kHz, 100 kHz, 1 MHz and 10 MHz. The loss tangent was also determined during the weak-field tests. The relative permittivity and loss tangent are plotted as a function of temperature and frequency within the a-b plane in Fig. 8 and along the c-axis in Fig. 9.

The Curie temperature of BTO has been previously shown to be 675°C [23]. That transition is visible at slightly lower temperatures, about 660°C, likely due to the proximity of the thermocouple to the sample. The loss tangent at lower frequencies is larger than that at higher frequencies for the same temperature, indicating that conduction mechanisms are frequency dependent, as shown in prior work [7, 10]. The effect of the conduction mechanisms can be mitigated by increasing the measurement frequency, but even at the highest frequencies measured, the loss becomes significant by about 300°C [10, 23]. The frequency dependence of the measurements indicates the difficulty of comparing work within the literature, as measurements are typically not taken at the same frequency and are therefore difficult to compare. The loss tangent increases with increasing temperature, which is consistent with the onset of conduction mechanisms previously discussed. Additionally, the loss tangent is higher within the a-b plane for a given set of test conditions, indicating that conduction is greater within the

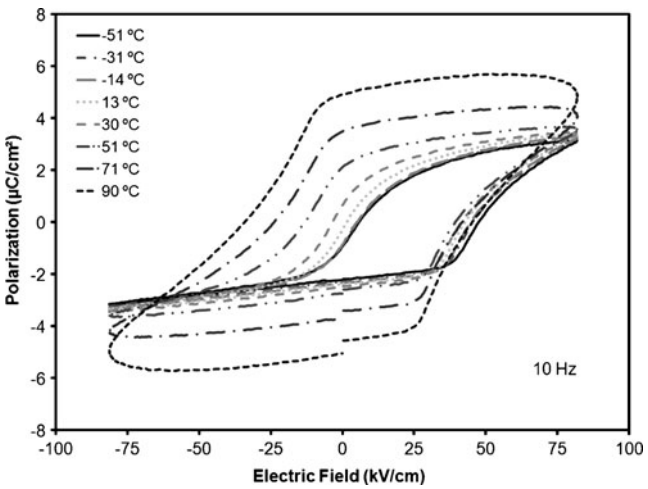

Fig. 7 Effect of temperature on the polarization along the c-axis of a textured sample measured at 10 Hz

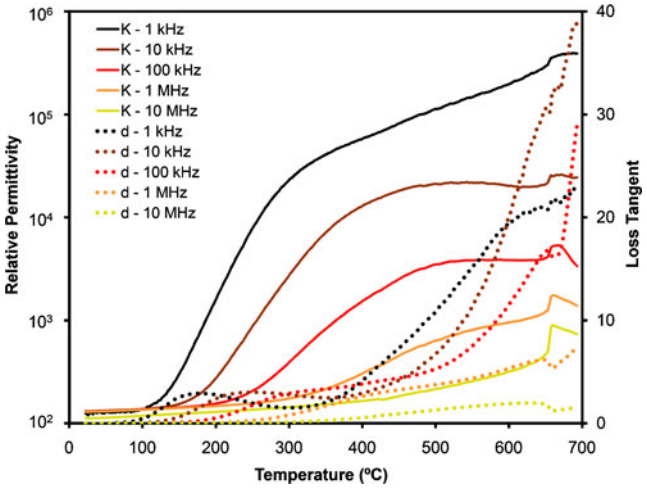

Fig. 8 Relative permittivity and loss tangent as a function of temperature and frequency for textured BTO measured within the a-b plane

a-b plane [10, 11]. The large loss due to conduction within the material is not unexpected. Previous work on single crystals has shown that BTO has a high electrical conductivity within the polarization plane [23]. Fortunately, previous work has also shown that loss mechanisms are mitigated by doping with Group V and VI elements, and it is likely that such doping would have a similar effect and delay the onset of conduction within BTO textured by screen printing [24, 25, 28, 29].

The room temperature relative permittivity within the a-b plane is approximately 130, which corresponds to previous work on textured BTO and slightly lower than expected from single crystal measurements [3, 7, 10, 23]. The room temperature relative permittivity along the c-axis is approximately 110, which is comparable to previous work and somewhat lower than the single crystal value of 140 [3, 7, 10, 13, 23]. The large increase in relative permittivity concurrent with the increase in loss is due to conduction within the material and not representative of the true relative permittivity.

To compare the effect of orientation on the relative permittivity, measurements taken at 1 MHz along the c-axis and within the a-b plane were compared to a random sample, shown in Fig. 10.

Initially, the relative permittivity within the a-b plane is only slightly higher than along the c-axis and the randomly oriented sample. However, the differences due to crystallographic texture become apparent as the temperature increases, with a very distinct augmentation of the relative permittivity within the a-b plane as compared to the randomly oriented sample. As expected, the relative permittivity along the c-axis is lower than that of the random sample and much lower than that measured within the a-b plane, demonstrating that crystallographic texture can drastically improve the relative permittivity of BTO.

The electrical results demonstrate that inducing crystalline texture may have secondary results, such as conductivity enhancement. While the conductivity increase can be mitigated with doping, unintended consequences of texturing must be considered when assessing the value of these materials as replacements for lead-based systems. Furthermore, other properties such as thermal conductivity and mechanical properties are influenced by crystalline texture [30]. Concurrent property enhancement may in fact become a useful feature if texture anisotropy is leveraged. Anisotropic thermal conductivity, for example, would be very useful if successfully combined with integrated electronics, as thermal management becomes a larger issue with decreasing device footprint. Several other applications may also benefit from engineered directional properties,

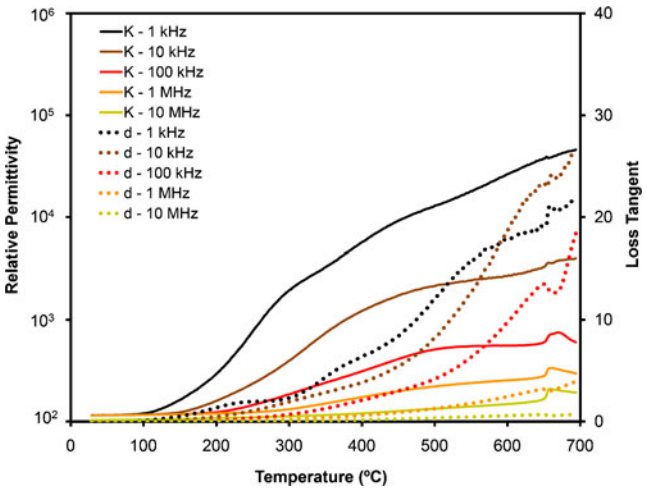

Fig. 9 Relative permittivity and loss tangent as a function of temperature and frequency for textured BTO measured along the c-axis

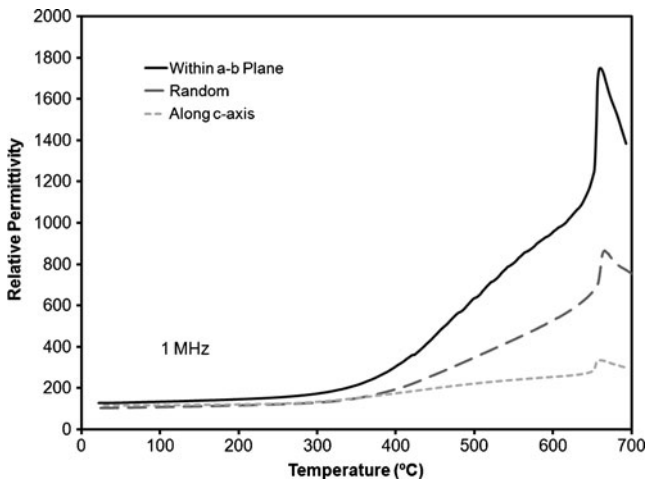

Fig. 10 Effect of orientation on the relative permittivity as a function of temperature measured at 1 MHz

such as thermal barrier coatings having anisotropic thermal conductivity or directional mechanical properties.

4 Conclusions

The enhancement of electrical properties obtained through screen printing is comparable to those obtained with other texturing techniques such as hot forging and tape casting. The electrical properties have been shown to be highly dependent on measurement frequency, temperature and even the electrical field history of the sample. Conduction is enhanced via the defect chemistry of textured BTO and is frequency and temperature dependent. These are all important considerations when determining the potential of textured BTO to replace lead-based dielectrics.

Acknowledgements Sandia is a multi-program laboratory operated by Sandia Corporation, a Lockheed Martin company, for the United States Department of Energy's National Nuclear Security Administration under contract DE-AC04-94AL85000.

References

1. T.R. Shrout, S.J. Zhang, J. Electroceram. **19**, 111–124 (2007)
2. S.J. Zhang, R. Xia, T.R. Shrout, J. Electroceram. **19**, 251–257 (2007)
3. T. Takenaka, K. Sakata, Jpn. J. Appl. Phys. **19**, 31–39 (1980)
4. Y. Kinemuchi, P.H. Xiang, H. Kaga, K. Watari, J. Am. Ceram. Soc. **90**, 2753–2758 (2007)
5. P.A. Fuierer, A. Nichtawitz, Proc. 9th IEEE Int. Symp. Appl. Ferroelectr. 126–129 (1994)
6. J.A. Horn, S.C. Zhang, U. Selvaraj, G.L. Messing, S. Trolier-McKinstry, J. Am. Ceram. Soc. **82**, 921–926 (1999)
7. Y.M. Kan, P.L. Wang, Y.X. Li, Y.B. Cheng, D.S. Yan, J. Eur. Ceram. Soc. **23**, 2163–2169 (2003)
8. T. Kimura, T. Yoshimoto, N. Iida, Y. Fujita, T. Yamaguchi, J. Am. Ceram. Soc. **72**, 85–89 (1989)
9. J.S. Patwardhan, M.N. Rahaman, J. Mater. Sci. **39**, 133–139 (2004)
10. V.K. Seth, W.A. Schulze, IEEE T. Ultrason. Ferr. Freq. Control **36**, 41–49 (1989)
11. S. Swartz, W.A. Schulze, J.V. Biggers, Ferroelectr. **38**, 765–768 (1981)
12. H. Watanabe, T. Kimura, T. Yamaguchi, J. Am. Ceram. Soc **72**, 289–293 (1989)
13. P.H. Xiang, Y. Kinemuchi, K. Watari, J. Eur. Ceram. Soc **27**, 663–667 (2007)
14. J.J. Hao, X.H. Wang, R.Z. Chen, Z.L. Gui, L.T. Li, J. Am. Ceram. Soc. **87**, 1404–1406 (2004)
15. H. Watanabe, T. Kimura, T. Yamaguchi, J. Am. Ceram. Soc. **74**, 139–147 (1991)
16. M.J. Wu, Y.X. Li, D. Wang, J.T. Zeng, Q.R. Yin, J. Electroceram. **22**, 131–135 (2009)
17. Y. Saito, H. Takao, T. Tani, T. Nonoyama, K. Takatori, T. Homma, T. Nagaya, M. Nakamura, Nat. **432**, 84–87 (2004)
18. M.R. Winter, C.B. DiAntonio, P. Yang, M.A. Rodriguez, J.R. Michael, T.P. Chavez, B.B. McKenzie, J. Am. Ceram. Soc. **93**, 1922–1926 (2010)
19. S.E. Cummins, L.E. Cross, J. Appl. Phys. **39**, 2268–2274 (1968)
20. M. Holmes, R.E. Newnham, L.E. Cross, Am. Ceram. Soc. Bull. **58**, 872 (1979)
21. S.K. Kim, M. Miyayama, H. Yanagida, Mater. Res. Bull. **31**, 121–131 (1996)
22. T. Kimura, T. Yamaguchi, Ceram. Int. **9**, 13–17 (1983)
23. A. Fouskova, L.E. Cross, J. Appl. Phys. **41**, 2834–2838 (1970)
24. S.H. Hong, J.A. Horn, S. Trolier-McKinstry, G.L. Messing, J. Mater. Sci. Lett. **19**, 1661–1664 (2000)
25. H.S. Shulman, M. Testorf, D. Damjanovic, N. Setter, J. Am. Ceram. Soc. **79**, 3124–3128 (1996)
26. R.A. Eichel, J. Electroceram. **19**, 9–21 (2007)
27. K. Carl, K.H. Hardtl, Ferroelectr. **17**, 473–486 (1978)
28. S.H. Hong, S. Trolier-McKinstry, G.L. Messing, J. Am. Ceram. Soc. **83**, 113–118 (2000)
29. S.S. Lopatin, T.G. Lupeiko, T.L. Vasiltsova, N.I. Basenko, I.M. Berlizev, Inorg. Mater. **24**, 1328–1330 (1988)
30. Y. Shen, D.R. Clarke, P.A. Fuierer, Appl. Phys. Lett. **93**, 102907 (2008)